Available online at www.sciencedirect.com
SCIENCE DIRECT®
ELSEVIER
Nuclear Instruments and Methods in Physics Research A 553 (2005) 592–603
NUCLEAR INSTRUMENTS & METHODS IN PHYSICS RESEARCH Section A
www.elsevier.com/locate/nima

Monte-Carlo simulations of small angle neutron scattering instruments at European spallation source

K. Lieutenant[a,b,*], T. Gutberlet[a,c], A. Wiedenmann[a], F. Mezei[a,d]

[a]*Hahn-Meitner-Institut Berlin, Glienicker Str. 100, D-14109 Berlin, Germany*
[b]*Scientific Computing, Institut Laue-Langevin, 6 rue Jules Horowitz, F-38000 Grenoble, France*
[c]*Laboratory for Neutron Scattering, Paul Scherrer Institut, CH-5232 Villigen PSI, Switzerland*
[d]*LANSCE, Los Alamos National Laboratory, Los Alamos, NM 87545, USA*

Received 21 September 2004; received in revised form 17 January 2005; accepted 19 May 2005
Available online 6 July 2005

Abstract

Monte-Carlo simulations of small angle neutron scattering (SANS) instruments have been performed using the VITESS software package in order to investigate the performance of such neutron spectrometers at high-power spallation sources as European spallation source (ESS).

The performed simulations show that a low Q-range SANS instrument down to $Q = 3 \times 10^{-4}\,\text{Å}^{-1}$ can be suitably built using a 60 m free neutron flight path (30 m collimation length and 30 m sample to detector distance) and a wavelength range up to 20 Å. Free neutron flight paths of 30 and 4 m with wavelength ranges of 4.6–6.5 and of 4.6–10 Å cover accessible Q-ranges of 2×10^{-3}–6×10^{-2} and 2×10^{-2}–$0.45\,\text{Å}^{-1}$, respectively, with fair resolution and large overlap regions. The total length of the instrument would be 66 m from source to detector. Instruments with significantly larger neutron flight paths show no further gain in its performance.

Highest count rates were received at the proposed long pulse target station of ESS with up to an order of magnitude intensity gain compared to the proposed short pulse target station of ESS or the ILL as neutron source in the three wavelength ranges anticipated.

PACS: 02.70.Uu; 29.25.Dz; 61.12.Ex

Keywords: MC simulation; Neutron sources; Spallation source; SANS

1. Introduction

Small angle neutron scattering (SANS) is one of the most powerful and requested techniques in elastic neutron scattering serving scientific interests

*Corresponding author at: Scientific Computing, Institut Laue-Langevin, 6 rue Jules Horowitz, F-38000 Grenoble, France. Tel.: +33 476 20 78 03; fax: +33 476 20 76 48.
E-mail address: lieutena@ill.fr (K. Lieutenant).

0168-9002/$ - see front matter © 2005 Published by Elsevier B.V.
doi:10.1016/j.nima.2005.05.053

in biology, chemistry, physics and material sciences, investigating colloids, polymers, metal alloys, magnetic systems, superconductors, porous materials, minerals and many others. Objects in the range of a few nanometre in diameter up to several hundred nanometre can be investigated and their aggregation and/or growth studied under various conditions and environments. Most important in situ studies of reactions and dynamics via structural changes can be performed within a wide Q-range with single experiments at short times.

Time-of-flight SANS at high-power spallation neutron sources as those under construction in the US and Japan and proposed for Europe will offer many new opportunities in the various areas of research using SANS due to increased count rates, improved resolution and expanded Q-range offered by flexible state-of-the-art pulsed neutron source SANS machines. The higher flux anticipated will permit smaller quantities and lower concentrations of precious samples to be used.

In order to define the design parameters for such flexible state-of-the-art SANS instruments at future spallation neutron sources dedicated, Monte-Carlo simulations offer the opportunity to simulate instrument performances depending on the available source characteristic. With respect to the proposed European spallation source (ESS) such an instrument can be operated at two different target stations considered: (i) a short pulse spallation source (SPSS) with 50 Hz repetition rate and 5 MW beam power; and (ii) a long pulse spallation source (LPSS) with 16.67 Hz repetition rate and 5 MW beam power. As SANS measurements do not require high time or wavelength resolution but a broad neutron wavelength band with an intensity as high as possible especially at high neutron wavelength, the preferable moderator to be viewed at by the instrument at the source would be a cold-coupled moderator. The performance of a cold-coupled moderator has been described for the ESS target stations [1].

As requested for the investigation of larger aggregates, e.g. in biology or colloid sciences the design of a dedicated SANS instrument has to be able to cover a Q-range of at least 10^{-3}–$0.4\,\text{Å}^{-1}$. Usually, SANS measurements are performed in the range $0.3 < QR_0 < 20$, which results in a maximum for the diameter of objects to be studied of about 2000 Å with most current instruments. A maximal diameter R_0 of 6670 Å or 0.667 μm, which is already in the range of visible light, would be reached extending the accessible Q-range to lower values close to $3 \times 10^{-4}\,\text{Å}^{-1}$.

The performance of such an SANS instrument in pinhole geometry installed on an optimal source might serve as a standard to value new approaches to reach very low Q-values like focussing mirrors [2], lenses [3], sextupoles [4], multiple grids [5] or double-monochromator-based USANS instruments [6].

Furthermore, the performance of such an SANS machine must be compared with and outperform an instrument at the best existing source of cold neutrons, the ILL. In addition, it should take into account current concepts for SANS instruments at the American spallation neutron source SNS and the Japanese spallation source JSNS currently under construction.

In the present report, Monte-Carlo simulations on the performance of a time-of-flight SANS instrument at the proposed target stations of the ESS are presented and compared with its performance at the ILL neutron source. At first the analytical considerations for the simulations regarding moderators, neutron guide, chopper and detectors systems will be described. Next, details of the Monte-Carlo simulation procedures are given; finally, a comparison of the obtained results with respect to neutron guide and chopper characteristics is presented, taking into account different neutron sources and different instrument layouts.

2. Analytical considerations for the SANS set-up

2.1. General layout

The sizes of guide, sample, beam-stop, and detector as well as the positions of sample and two of the three choppers are kept fixed. Only the free flight path is variable, which is realised by removable guides, a movable detector and a movable wavelength band chopper of the instruments on pulsed sources (see Fig. 1, Tables 1 and

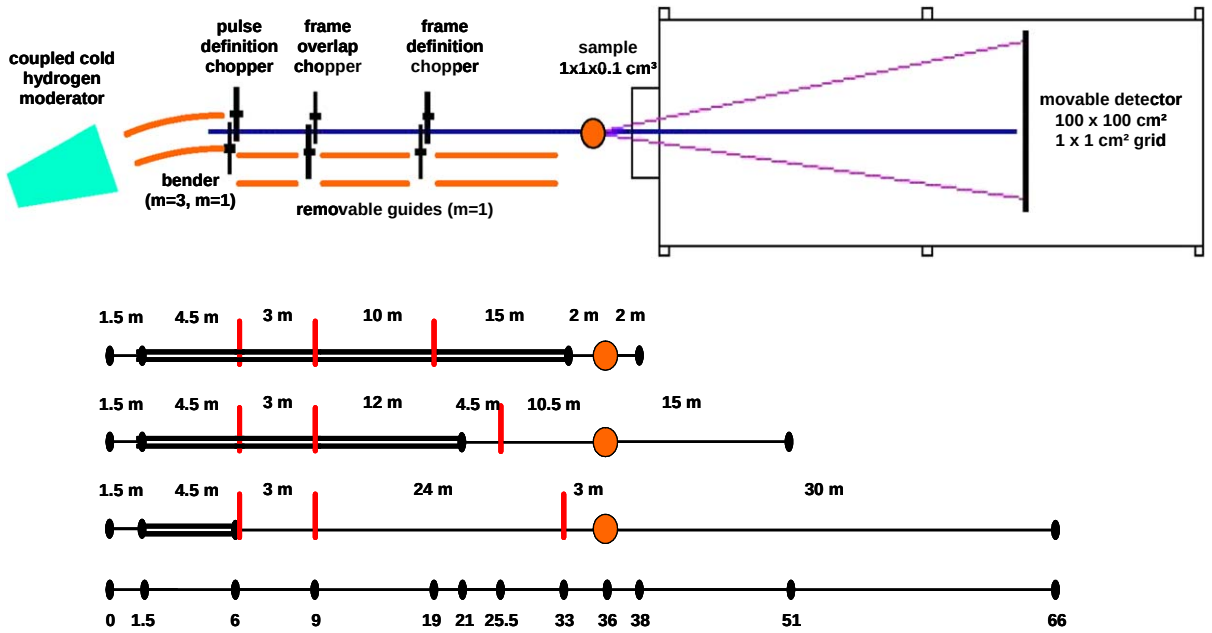

Fig. 1. Scheme of the instruments: the instruments considered start at the position of the moderator. The first chopper (vertical bar) is placed at the end of the target shielding, 6 m from the moderator. The sample (ellipse) is situated at a fixed position 36 m from the moderator followed by a PSD system. The free flight paths (single lines) are 2, 15 and 30 m before the sample and the same distance behind the sample. These three set-ups are shown on the bottom of the figure. The variation is achieved by removable guides (double lines) and a movable detector. A 180° wavelength band chopper is positioned half-way between moderator and detector. A frame overlap chopper is placed 9 m from the moderator. In the drawing of the three set-ups, relative distances between components are shown, whereas the last line shows distances from the moderator for all three set-ups.

Table 1
Data of the simulation of the instrument set-ups at pulsed sources

	6–30–30 m	21–15–15 m	34–2–2 m	6–15–15 m	6–45–45 m
Source 0.0 m	ESS LPSS\SPSS	ESS LPSS\SPSS	ESS LPSS\SPSS	ESS LPSS	ESS LPSS
Curved guide $3 \times 3\,cm^2$, $m = 3$	1.50–5.97 m	1.50–5.97 m	1.50–5.97 m	1.50–5.97 m	1.50–5.97 m
Double chopper 5.97–6.03 m	50.2°	59°	67°	70°	35.5°
Guide $3 \times 3\,cm^2$, $m = 1$		6.03–8.97 m	6.03–8.97 m		
Double chopper 8.97–9.03 m	65°\64.5°	78.5°\78°	99.5°\98°	102°	51°
Guide $3 \times 3\,cm^2$, $m = 1$		9–21 m	9–19 m		
Double chopper 180°	32.97–33.03 m	25.47–25.53 m	18.97–19.03 m	17.97–18.03 m	47.97–48.03 m
Guide $3 \times 3\,cm^2$, $m = 1$			19.03–34.00 m		
Aperture $1 \times 1\,cm^2$	at 35.99 m	at 35.99 m	at 35.99 m	at 20.99 m	at 50.99 m
Sample $1 \times 1 \times 0.1\,cm^3$ ($W \times H \times T$)	at 36.00 m	at 36.00 m	at 36.00 m	at 21.00 m	at 51.00 m
Beamstop $5 \times 5\,cm^2$	at 65.95 m	at 50.95 m	at 37.95 m	at 35.95 m	at 95.95 m
Detector $100 \times 100\,cm^2$ grid $1 \times 1\,cm^2$	at 66.00 m	at 51.00 m	at 38.00 m	at 36.00 m	at 96.00 m

Note: All positions are measured from the source. For the choppers, the widths of the apertures are given (in deg.). A coupled hydrogen moderator is used in all cases.

Table 2
Data of the simulation of the instrument at the reactor source

	6–30–30 m	21–15–15 m	34–2–2 m
Source 0.0 m	ILL cold	ILL cold	ILL cold
Curved guide $3 \times 3\,cm^2$, $m = 3$	1.50–5.97 m	1.50–5.97 m	1.50–5.97 m
Velocity selector 5.97–6.24 m 10% FWHM 72 chan., 52.2°	118.7 rps	425.4 rps	425.4 rps
Aperture $3 \times 3\,cm^2$	at 6.24 m		
Guide $3 \times 3\,cm^2$, $m = 1$		6.24–21.24 m	6.24–34.24 m
Aperture $1 \times 1\,cm^2$	at 36.23 m	at 36.23 m	at 36.23 m
Sample $1 \times 1 \times 0.1\,cm^3$ (W × H × T)	at 36.24 m	at 36.24 m	at 36.24 m
Beamstop $5 \times 5\,cm^2$	at 66.19 m	at 51.19 m	at 38.19 m
Detector $100 \times 100\,cm^2$ grid $1 \times 1\,cm^2$	at 66.24 m	at 51.24 m	at 38.24 m

Note: For the wavelength selector, the twisting angle of a blade over its whole length is given. A hydrogen moderator is used in all cases.

2). Additionally, the chopper apertures of the first two choppers are supposed to be variable.

The guide system starts 1.5 m from the moderator. A 4.5 m long bender is installed inside the shielding to get out of direct view of the source. After 6 m, the first chopper is placed at the end of the target shielding. The sample is situated at a fixed position 30 m down the first chopper, followed by a position sensitive detector (PSD). The free flight paths are 2×2, 2×15 and $2 \times 30\,m^2$ with the same distance from guide to sample and from sample to detector. The variation is achieved by removable guide segments and a movable detector. A 180° wavelength band chopper is positioned half-way between the source and detector. A frame overlap chopper is placed 9 m from the moderator.

2.2. Moderators

To evaluate, which of the two target stations proposed for ESS yields best results, simulations with each of these two sources were performed. The moderator characteristics were used as published [1]. A maximal pulse length of $t_{p,max} = 2.7$ ms was considered for SPSS and a length of $t_{p,max} = 4.7$ ms for LPSS.

For comparison of the results with an existing source, simulations with equivalent parameters for the ILL reactor source were performed. The neutron flux distribution for the reactor source was taken from Ref. [1].

2.3. Instrument resolution

The momentum transfer Q depends on the scattering angle θ and the wavelength λ. For reactor sources, the wavelength resolution $\Delta\lambda/\lambda$ is directly determined by the geometry and performance of the velocity selector. For pulsed sources, the wavelength λ is calculated from the time-of-flight t. Therefore, the resolution in λ is a consequence of the pulse length t_p. The uncertainty $\Delta\theta$ of θ is given by the widths of the diaphragms and the spatial detector resolution. Both effects are independent of each other; thus, the resolution in Q is

$$r_Q = \Delta Q/Q = ((\Delta\lambda/\lambda)^2 + (\Delta\theta/\theta)^2)^{1/2}. \quad (1)$$

For small scattering angles (and small deviations), which is well fulfilled for SANS measurements, $\Delta\theta/\theta$ is independent of the flight path length $(L + L)$:

$$\left\langle \frac{\Delta\theta}{\theta} \right\rangle = \frac{\sqrt{\arctan^2\left(\frac{d_1+d_2}{4L}\right) + \arctan^2\left(\frac{d_2+\Delta D}{4L}\right)}}{\arctan\left(D/L\right)} \approx \frac{(d_1+d_2)^2 + (d_2+\Delta D)^2}{4D} \quad (2)$$

where d_1 is the size of aperture 1, d_2 the size of aperture 2, ΔD the detector grid, D the distance

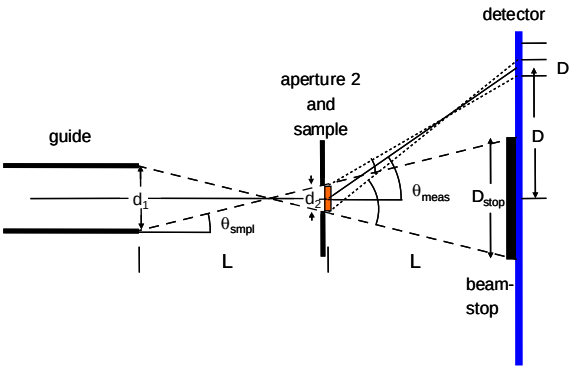

Fig. 2. Illustration of the maximal usable divergence θ_{smpl} (dashed lines) and the parameters causing the uncertainty in determining the scattering angle: The dotted lines indicate the paths with minimal and maximal possible scattering angle that contribute to the signal in a cell belonging to a scattering angle θ_{meas} (solid line). d_1 is the size of the first aperture or of the guide size, d_2 is the size of the second aperture, ΔD is the size of a cell of the detector grid. The minimal size of a beam-stop is shown in this drawing too.

between the place of detection and the centre of the detector (cf. Fig. 2). Therefore, all instruments simulated here have the same angular resolution, because the same aperture and detector sizes as well as the same detector grid are used in all simulations.

The wavelength resolution can be calculated by

$$\left\langle \frac{\Delta\lambda}{\lambda} \right\rangle = \frac{\Delta T}{T} \approx \frac{t_{\mathrm{p}} h/m_{\mathrm{n}}}{L\lambda} \tag{3}$$

where t_{p} is the pulse length which is the main contribution to the uncertainty in wavelength determination, h the Planck's constant, m_{n} the neutron mass. In the present simulations diaphragms of 3×3 and $1\times1\,\mathrm{cm}^2$ at the beginning and at the end of the collimation section were considered, a neutron guide of $3\times3\,\mathrm{cm}^2$ cross-section, a sample of $1\times1\,\mathrm{cm}^2$ size and a detector grid of $1\times1\,\mathrm{cm}^2$. As a consequence, the minimal size of the beam-stop is $5\times5\,\mathrm{cm}^2$ (cf. Fig. 2), to be used in the simulations. (Therefore $d_1 = 3\,\mathrm{cm}$, $d_2 = 1\,\mathrm{cm}$, $\Delta D = 1\,\mathrm{cm}$, $D_{\mathrm{stop}} = 5\,\mathrm{cm}$.) For the pulse length t_{p} at the SPSS a mean deviation of 0.3 ms was assumed and 0.8 ms at the LPSS (cf. Ref. [1]) to calculate the achievable instrument resolutions.

At the pulsed sources the wavelength resolution is by far better than the angular resolution, i.e. the total resolution is determined by the angular resolution for each point on the detector. At the continuous source the wavelength and the angular resolution are comparable (except close to the beam-stop). A calculation yields a resolution in Q of 44.7% directly at the beam-stop and about 2.3% at the corners of the detector for the instruments at ESS simulated here. For the instruments at the continuous source, the values are somewhat larger (44.9% and 4.8%).

2.4. Bender and guide layout

In order to suppress contamination by short wavelength neutrons (hot neutrons) in the wavelength band guided to the sample and to reach a useful signal-to-noise ratio, the neutron path is bent between the source and the first chopper placed in the instrument layout.

By the current ESS target design a neutron guide can be installed at a distance as close as 1.5 m to the source [7]. The biological shielding is ending at a distance of 6 m from the source. Therefore, this primary neutron guide can have only a length of $L = 4.5\,\mathrm{m}$ in which the beam can be bent out of direct beam view.

For small curvatures the radius R is calculated by

$$R = L^2/(8D) \tag{4}$$

where D is the outer width of the neutron guide. Assuming a wall thickness of 1 cm, one gets $D = 5\,\mathrm{cm}$ and $R = 50.6\,\mathrm{m}$ for a $3\times3\,\mathrm{cm}^2$ guide cross-section. In the simulations, a slightly smaller curvature for the neutron guide with a radius of 50 m was used.

This curvature causes an angle of reflection of

$$\theta_+ = a\,\tan[(2d_1R)^{1/2}/(R-\tfrac{1}{2}d_1)] \approx a\,\tan[(2d_1/R)^{1/2}] = 1.98^\circ \tag{5}$$

for neutrons entering without divergence at the inner side into the bending neutron guide (with d being the inner width of the neutron guide). This angle increases to 2.06° for neutrons with a divergence of 0.57° (see below).

In order to reflect all neutrons of the used wavelength bands (cf. Table 3), a supermirror

Table 3
Wavelength ranges usable for data evaluation at different sources for the set-ups examined

Source	6–30–30 m	21–15–15 m	34–2–2 m	6–15–15 m	6–45–45 m
LP (Å)	16.37–19.65	4.85–9.03	4.95–10.53	4.92–10.91	10.88–13.13
SP (Å)	18.66–19.68	4.68–5.99	4.71–6.45		
CW (Å)	16.20–19.80	4.50–5.50	4.50–5.50		

Note: The maximal time range at detector without overlap by succeeding pulses and half-shadow time is calculated and the corresponding wavelength range determined. Only neutrons arriving during this time have been considered in the data evaluation.

coating of at least

$$m = \frac{\theta_{\max}}{0.099^\circ\,\text{Å}^{-1} \times \lambda_{\min}} = \frac{2.06^\circ}{0.099^\circ\,\text{Å}^{-1} \times 4.5\,\text{Å}} = 4.62 \quad (6)$$

is required. Despite recent success in the production of supermirrors with $m > 5$ [8], the required amount of mirrors for a 4.5 m long guide is difficult to get and very expensive at the moment; therefore, we reduced the maximal angle. This is achieved by introducing channels in the bender, which diminish θ_+ by decreasing the width d_1 to half, a third, etc. of the original value (cf. Eq. (5)). One to three channels and supermirror coatings of $m = 2$, 3 and 3.5 were tested to find the optimal bender.

The maximal desirable divergence is given by the maximal angle under which neutrons can hit the sample after leaving the guide (see Fig. 2). For the set-up with the shortest flight path (2 m between end of guide and sample) and the given sizes d_1 and d_2 of the diaphragms, that is

$$\theta_{\text{smpl}} = a \tan\left(\tfrac{1}{2}(d_1 + d_2)/L\right) = 0.57^\circ. \quad (7)$$

Normal nickel allows a divergence of 0.446° for the shortest wavelength under consideration (4.5 Å), for ^{58}Ni this is 0.516°. This is already close to the maximal desirable divergence of 0.57°. Therefore, ^{58}Ni and normal nickel have been used as coatings of the various straight guides (along the beam path) in the simulations and no supermirror coating was tested. The results have been compared to find the best coating.

Currently, existing options and future improvements of neutron polarising devices should offer effective solutions to introduce polarised neutrons in the set-up of the future SANS instrument. But they have not been considered in the present simulations.

2.5. Monochromating and detector systems

For the definition of the allowed wavelength band a system of three counter-rotating double choppers has been assumed, each rotating with the frequency of the source. The first chopper has been situated as close as possible to the source, which is a distance of 6 m for the ESS target stations. The second chopper has been placed in a distance 1.5 times greater than the first one, i.e. 9 m. A third chopper, a wavelength band chopper of 180° has been placed half-way between source and detector in all settings.

Choppers of 35 cm radius with a distance of 5.2 cm between the double chopper discs and the axle positioned 33 cm from the centre of the guide were anticipated. Openings and phases of the frame overlap choppers were chosen in a way that they do not stop any neutron of the main part of the pulse ($t_{\text{start}} < 1.0$ ms (SPSS), $t_{\text{start}} < 2.5$ ms (LPSS)) that is able to pass the wavelength band chopper (see Fig. 3). The data of the choppers are collected in Table 1.

For the reactor source a velocity selector of 10% FWHM for mean wavelengths of 5.0 and 18.0 Å, respectively, was implemented in the simulations.

For the detector system, a standard two-dimensional system with an area of $100 \times 100\,\text{cm}^2$ and a grid of $1.0 \times 1.0\,\text{cm}^2$ with an assumed efficiency of 0.9 was defined.

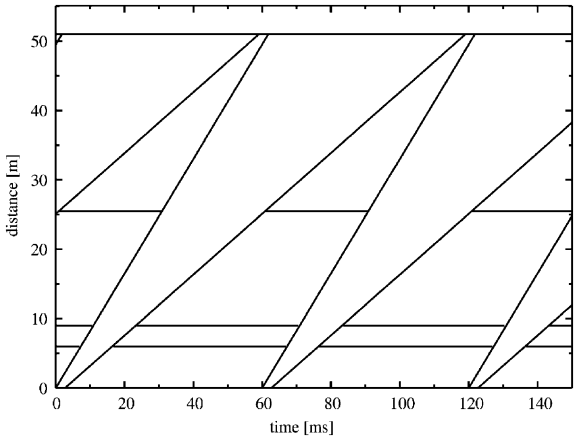

Fig. 3. Distance–time diagram of the (21 + 15 + 15) m set-up on the long pulse target station.

3. MC simulations and data evaluation

3.1. MC simulations

The simulations were performed with the VITESS software package [9,10]. Usually, 10^9 trajectories were started, 14,000–510,000 of which reached the sample. Each was scattered 10 times to improve statistics at the detector. All parameters of the simulations are summarised in Tables 1 and 2. The effect of gravity was not taken into account in the simulations.

The module sample_sans implemented in VITESS describes the small angle scattering of mono-disperse hard particles. If the trajectory hits the sample, it is scattered on its path through the sample at a certain distance L_s from its entrance, which is determined by a Monte-Carlo choice. The scattering is restricted to an angular range of $[\theta - \Delta\theta,\ \theta + \Delta\theta]$, $[\varphi - \Delta\varphi,\ \varphi + \Delta\varphi]$ by the input values for θ, $\Delta\theta$, φ and $\Delta\varphi$. The direction of the trajectory i behind the sample is given by (θ_i, φ_i), determined by a Monte-Carlo choice in these ranges.

For all trajectories, an attenuation A_t is considered as follows:

$$A_t = \exp\{-L_n(\mu_{tot} + \mu_{abs}\lambda/1.798\,\text{Å})\} \tag{8}$$

where L_n is the total neutron flight path in the sample (surface → point of scattering → surface). μ_{tot} denotes the (wavelength independent) total macroscopic scattering cross-section, μ_{abs} is the macroscopic absorption cross-section (to be provided for $\lambda = 1.798$ Å).

3.2. Data evaluation

Using a 180° chopper half-way between source and detector, an overlap region is caused, where neutrons of two successive pulses arrive. The neutrons arriving in this time interval are not considered in the data evaluation. Therefore, a so-called 'time-of-evaluation' is calculated. The beginning of the time is calculated from the time-of-flight for the longest wavelength λ_{max} of the previous pulse. The end of the time interval is determined by the shortest wavelength of the following pulse (starting at $t_{p,max}$). Additionally, those neutrons passing the wavelength band chopper during the time T_{HS} when it is opening or closing (half-shadow) are suppressed by reducing further the time-of-evaluation:

$$t_{min} = L_{ges} m_n \lambda_{max}/h - T + T_{HS} \tag{9a}$$

$$t_{max} = L_{ges} m_n \lambda_{min}/h + T - T_{HS} + t_{p,max} \tag{9b}$$

with T pulse repetition time, L_{ges} as the distance source to detector, m_n the mass of a neutron and h Planck's constant. From the resulting time intervals, the usable wavelength range was calculated (see Table 3).

All neutrons hitting one cell of the detector were treated like having hit the centre of that grid and having left the sample at its centre. In the case of the reactor source, the wavelength is thought to be the wavelength of the velocity selector used, i.e. 5 or 18 Å. For the spallation sources it is calculated from the time-of-flight starting at the beginning of the pulse. From these values, the momentum transfer is calculated and the results are shown as the count rate at the detector as a function of momentum transfer.

4. Results and discussion

4.1. Quality and performance of guides and bender

Taking the neutron spectrum of the ILL source as a reference, the performances of the straight neutron guides coated with normal Ni and with ^{58}Ni were compared. Using the instrumental set-up with 38 m total length, the flux at the sample is 7.7% higher with ^{58}Ni, but the flux leaving the guide is 31.2% higher. The reason is that neutrons that are transported in ^{58}Ni guides and not in normal nickel guides have a higher divergence (than accepted by nickel). They usually do not contribute to the flux at the sample because they do not hit it in a SANS instrument—except for very short wavelengths for which the maximal divergence is low.

As these neutrons reduce the signal-to-noise ratio for all instrument layouts and the higher divergence is only useful for the design with the smallest guide to sample distance of 2 m, it is more favourable to use normal Ni only for the coating of the neutron guides.

By passing through a curved guide, the divergence of neutrons is changed (depending on the quality of the used mirrors). Therefore, the performance of benders with different supermirror coatings and different numbers of channels was examined by simulations varying the 6–30–30 m set-up of the reactor source. Coatings used were (a) $m = 2$, reflectivity for $m\theta_c$: $r(m\theta_c) = 0.9$, (b) $m = 3$, $r(m\theta_c) = 0.8$ and (c) $m = 3.5$, $r(m\theta_c) = 0.7$. The blade width between the channels in the bender was set to 0.5 mm. The highest neutron flux in the centre of the bender was achieved with two channels, using coatings with $m = 3$ or 3.5 (see Fig. 4). As a coating of $m = 3$ is less expensive, this is the more favourable solution; it was used in all following simulations.

Coating with $m = 3.5$ for bender and neutron guides was used in the design of the proposed BRIMS machine [11] and the SNS extended Q-range SANS [12]. For the second instrument best performance was simulated with a 10-channel bender of cross-section of $4 \times 4\,\mathrm{cm}^2$ of radius $R = 65$ m.

Furthermore, we analysed if an additional straight neutron guide after the bender is useful as discussed in the description of the SNS SANS machines [10,11]. Straight guides of 1, 2 and 3 m were used and compared to the performance without such a neutron guide. Less than 5 cm from the centre of the beam-line, no difference in intensity as a function of the horizontal position was found (not shown here). So, no additional straight neutron guide was set after the bender.

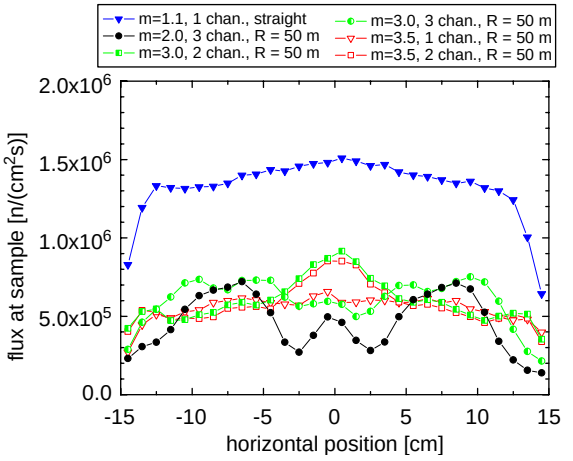

Fig. 4. Flux at the sample for different coatings and bender options of the (21 + 15 + 15) m set-up of the instrument at the reactor source.

4.2. Frame overlap

The chopper system anticipated suppresses frame overlap very effectively. The desired wavelength band of the neutrons passing the chopper system matches very well with the theoretical bandwidth listed in Table 3. Up to 50 Å, no neutrons of another frame were found in the simulations with the LPSS of the ESS. For the SPSS station, a small band of neutrons around 25 Å above the desired band did pass. By the proper adjustment of the chopper positions not done in the course of our simulations, this overlap can be avoided and has to be taken into account when building such an instrument.

4.3. Evaluation of the instrument layout

The present Monte-Carlo simulations were performed using a sample that scatters isotropicly

into all directions (see Fig. 5) and SANS samples of spherical particles of 100 and 1000 nm diameter (see Fig. 6) for three different layouts of the instrument considered. Count rates at the detector are shown as a function of momentum transfer Q. In all cases, a logarithmic binning was chosen, i.e. a bin is defined by a fixed value Q_{max}/Q_{min}, in this case $Q_{max}/Q_{min} = 1.04$. (Note that this kind of binning significantly influences the shape of the functions shown here.) The isotropic scattering reflects the moderator characteristics. In a real measurement, these characteristics have to be taken into account to evaluate the parameter $S(Q)$ from the raw data $I(Q)$ shown here.

The results show that a Q-range from 3×10^{-4} to 0.4 $Å^{-1}$ is covered with large overlap regions. At the low-Q end ($Q = 3 \times 10^{-4}$ $Å^{-1}$), count rates of a few hundred counts per seconds in a binning of $\Delta Q/Q = 0.04$ are simulated for samples of 1000 nm diameter.

Changing the set-up to 15 m collimation and 15 m sample–detector distance, the instrument performs well for spherical samples of 100 nm diameter. Due to the better resolution of the high-Q end of each spectrum, the minima in the SANS spectra are much more distinct than in the set-up with 2 m collimation and 2 m sample–detector distance. But for samples of 1000 nm diameter, the long 30 m collimation and sample–detector set-

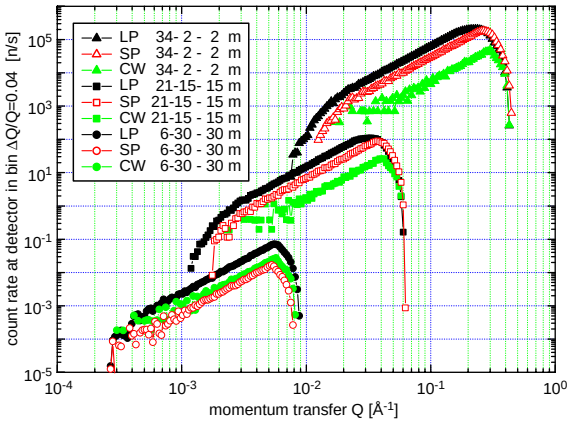

Fig. 5. Neutron count rate at the detector as a function of Q for SANS instruments at different sources and different instrument lengths using an isotropic scattering sample (10% of neutrons scattered).

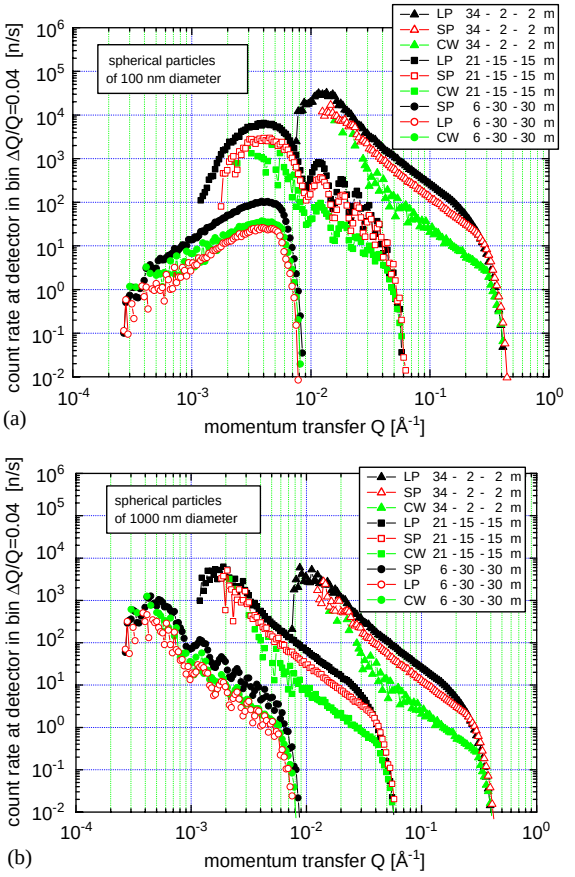

Fig. 6. Neutron count rate at the detector as a function of Q for SANS instruments at different sources and different instrument lengths using a sample with spherical particles of 100 nm (a) and 1000 nm (b) diameter.

up is necessary. For the same reasons as mentioned before, the minima are by far more distinct than in the set-up with 15 m collimation and sample–detector distance.

These three instrument settings are only basic examples; intermediate distances and wavelength ranges are accessible by the instrument layout. Thus, dedicated resolution and intensity ranges can be arranged for any distinct sample within its Q-range of interest.

4.4. Comparison of different instrument layouts

For a SANS machine at the SPSS of ESS, Heenan et al. [13] proposed a set-up with free flight

paths of (2+2) and (15+15) m with a wavelength range from 4.6 Å upwards. As the minimum measurable momentum transfer is given by

$$Q_{\min} = \frac{4\pi \sin(\theta)}{\lambda_{\max}} \approx \pi b(L_2 \lambda_{\max}) \quad (10)$$

where b is the diameter of beam-stop. $Q_{\min}$ reaches for such a set-up

$$Q_{\min} = \frac{\pi 0.05\,\mathrm{m}}{15\,\mathrm{m} \times 11.2\,\mathring{\mathrm{A}}} = 9.35 \times 10^{-4}\,\mathring{\mathrm{A}}^{-1} \quad (11)$$

which is a value reached for most SANS machines currently in operation. The present simulations show an easily reachable $Q_{\min}$ of $3 \times 10^{-4}\,\mathring{\mathrm{A}}^{-1}$ for an instrument of 66 m total length using a wavelength range up to 20 Å.

Because of the greater total length, the usable wavelength bands are reduced in the 21–15–15 m set-up in comparison to the instrument originally proposed (6–15–15 m), e.g. from 4.9–10.9 to 4.9–9.0 Å for the LPSS (cf. Fig. 3, Table 3). This results in a loss of intensity in the low-Q domain of the spectrum and a higher cut-off value—the minimal Q-value is $1.2 \times 10^{-3}\,\mathring{\mathrm{A}}^{-1}$ instead of $1 \times 10^{-3}\,\mathring{\mathrm{A}}^{-1}$ (see Fig. 7). Nevertheless, this reduced Q-range seems to be acceptable, because the 6–30–30 m set-up yields a by far higher resolution below $5 \times 10^{-3}\,\mathring{\mathrm{A}}^{-1}$ (cf. Fig. 6b). Above $3 \times 10^{-3}\,\mathring{\mathrm{A}}^{-1}$, the spectra are practically identical in intensity and resolution (see Fig. 7).

With a free flight path of 60 m, the centre of the beam at the detector is shifted downwards by $d = (36.6 \pm 3.6)$ cm for $\lambda = (18 \pm 0.9)\,\mathring{\mathrm{A}}$ due to the influence of gravity. (The effect is by far less distinct for the other set-ups.) In the current simulation, this effect is neglected, because this error can be corrected in the data evaluation routine for a TOF instrument. (The influence has been investigated in detail in a recent MC simulation study [14].) For instruments on continuous sources, this effect can be corrected by using prisms [15]. According to this idea, the wavelength dependence of the index of refraction is used to focus the beam on the detector. (Of course, prisms could also be used for SANS instruments on pulsed sources, but the correction of this effect in the data evaluation is the easier solution.) If it is not corrected, the wavelength

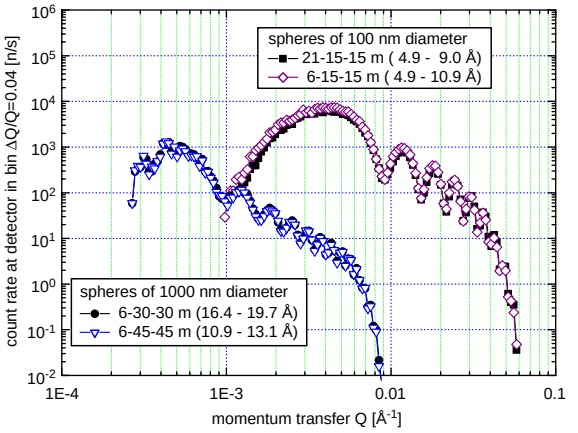

Fig. 7. Comparison of count rates at the detector of the LPSS for (15+15) m flight paths in instruments of different total length using a sample with spheres of 100 nm diameter, and with different flight paths (30+30 and 45+45 m), but the same range in momentum transfer Q (realised by adjusting the wavelength ranges) for spheres of 1000 nm diameter.

dependence of the shift reduces the resolution (in this case of very low Q-values), because it exceeds the cell size of the detector grid.

Assuming that the instrument might have a better performance with an even longer flight path (6–45–45 m) using an intermediate wavelength range around 12 Å, we also performed simulations with such a set-up. The angular resolution is identical as already shown in Section 2.3. In this case, also the wavelength resolution is identical, because the length L is enlarged by a factor 1.5 and the average wavelength λ reduced by a factor 1.5; thus, the product $L \times \lambda$, determining the wavelength resolution, is identical (see Eq. (3)).

The comparison of intensities obtained by the MC simulations also shows no significant differences (see Fig. 7). The disadvantages for set-ups with shortened flight paths (see above) grow with increasing total length of the instrument. Thus, a better performance is achieved by the set-up with a 66 m total length compared to that of 96 m. For the given characteristics of the ESS LPSS and the sizes of guide, apertures and beam-stop used in these simulations, there seems to be an optimal length of about 55–75 m, while much longer instruments show no advantage any more.

4.5. Comparison of the sources and target stations

For all set-ups simulated, the usable wavelength range is broadest at the long pulse station (LPSS, see Table 3). Therefore, the intensity is highest for each set-up (cf. Figs. 5 and 6). For an SANS instrument dedicated to reach Q-values significantly below $\times 10^{-3}\,\text{Å}^{-1}$ the LPSS is the best choice.

If a comparable instrument on a reactor source is set to a wavelength resolution of 10%, the usable wavelength band is smaller than at the LPSS in the short wavelength range. In the long wavelength range, the bandwidth becomes comparable (cf. Table 3). Therefore, a much higher intensity is reached using the 34–2–2 m set-up and the 21–15–15 m set-up, whereas the difference gets by far smaller approaching the low-Q end. A similar result was found in an earlier simulation [16]. Nevertheless, a factor in gain of intensity of about 2 remains (see Figs. 5 and 6).

On the SPSS, a much smaller wavelength band is usable. As a consequence, the intensity is smaller than that of the instrument on the reactor source for the 6–30–30 m option. But the resolution of the instrument on the reactor source is worse compared to instruments on either the SPSS or the LPSS spallation sources. In summary, the performance of such an SANS instrument at ESS would be better than at any existing reactor source, especially if it is installed at the LPSS.

4.6. Comparison with ILL and SNS SANS instruments

D22 at ILL is currently the SANS instrument with highest flux world wide; it is capable of covering a Q-range of 4×10^{-4}–0.44 (or $0.85\,\text{Å}^{-1}$ using the option to offset the detector system). The simulations show that the proposed SANS instrument for the ESS source has a gain in the count rate of about an order of magnitude compared to an instrument at the ILL source for the 34–2–2 and the 21–15–15 m set-up (see Fig. 5). These set-ups can be used for Q above $4 \times 10^{-3}\,\text{Å}^{-1}$ for all sources, for the spallation sources for even smaller Q values (if no high resolution is required). With the 6–30–30 m set-up, the instrument at the reactor source is competitive to those on spallation sources, but the count rate at the LPSS station is still higher in comparison to the ILL source down to $5 \times 10^{-4}\,\text{Å}^{-1}$, setting the proposed new instrument as the machine with highest flux and largest Q-range.

At SNS the extended Q-SANS instrument is designed to cover a Q-range from 0.004 to $12\,\text{Å}^{-1}$ with a wavelength bandwidth of 3.5–4.3 Å at different settings of the collimation and sample/detector distance. The high Q-values are reached by an additional high angle detector bank 1 m away from the sample position [12]. Similar instruments are proposed for JSNS: Hi-Resolution and Hi-Intensity SANS (Q-ranges from 0.002 to 15 and 0.001 to $10\,\text{Å}^{-1}$, respectively, bandwidth 0.6–7 Å for Hi-Intensity SANS) [17]. The present simulation of a 66 m long SANS instrument at the LPSS shows accessible coverage in Q from 3×10^{-4} to $0.4\,\text{Å}^{-1}$. The maximum in Q should be able to be enlarged by either a larger detector, an offset of the detector unit or additional detector units if higher Q-values are requested, but $Q_{\max}$ will probably not exceed values above $1\,\text{Å}^{-1}$.

The proposed SANS instrument BRIMS was foreseen for the discussed long wavelength target station at SNS [11]. It would cover a Q-range from 6.2×10^{-4} to $0.785\,\text{Å}^{-1}$ depending on apertures, collimation and sample/detector distance chosen. A comparison of the calculated scattered intensity at BRIMS with D22 at ILL has shown significantly increased count rates between $Q = 3 \times 10^{-3}$ and $0.5\,\text{Å}^{-1}$, but not for lower Q-values. The instrument at LPSS will outperform BRIMS, because the count rates of the SANS instrument at the LPSS source are significantly higher compared to the ILL source in practically the whole Q-range investigated, at least from 5×10^{-4} to $0.4\,\text{Å}^{-1}$ (Figs. 5 and 6).

5. Summary

A time-of-flight SANS instrument with an accessible Q-range from 3×10^{-4} to $0.4\,\text{Å}^{-1}$ is feasible with acceptable count rates for large samples in the whole Q-range at a high-power spallation neutron source. The instrument will be

very flexible, using variable neutron flight paths and wavelength ranges which can be adapted to the specific requirements of the individual measurement. The extension of the instrument from 36 to 66 m total length causes little disadvantages in a small Q-range ($\approx 1\times10^{-3}$–2×10^{-3} Å^{-1}), but great advantages for even smaller momentum transfers. According to these simulations, instruments of lengths far beyond that do not give additional advantages any more.

Installed on the proposed ESS LPSS, the instrument performance would be by far better than that of any existing instrument and go beyond the instruments foreseen at the currently constructed spallation neutron sources. An adaptation of new approaches to reach very low Q-values by focussing (see Section 1) will add additional profits to the instrument performance (see, e.g. Ref. [2]), especially for high resolution and low Q-values [18].

Acknowledgements

This work has been supported by the SCANS network within the 'Improving human potential programme' of the European Commission under contract HPRI-CT-1999-500013. We like to thank E. Hoinkis for fruitful discussions.

References

[1] http://www.hmi.de/bereiche/SF/ess/ESS-moderators.pdf; http://www.hmi.de/bereiche/SF/ess/ESS_mod_pics.pdf.
[2] B. Alefeld, D. Schwahn, T. Springer, Nucl. Instr. and Meth. A 274 (1989) 210.
[3] T. Adachi, et al., in: G. Mank, H. Conrad (Eds.), Proceedings of the ICANS-XVI, FZ Jülich, Jülich, 2003, p. 363.
[4] J. Suzuki, et al., in: G. Mank, H. Conrad (Eds.), Proceedings of the ICANS-XVI, FZ Jülich, Jülich, 2003, p. 427.
[5] F. Mezei, in: D. Richter (Ed.), The ESS Project Vol. II, New Science and Technology for the 21st Century, ESS, Jülich, 2002, pp. 3–21.
[6] M. Hainbuchner, et al., Physica A 304 (2002) 220; S. Borbely, et al., Physica B 276–278 (2000) 138.
[7] G.S. Bauer, et al., in: The ESS Project Vol. III, Technical Report, ESS, Jülich, 2002 (Chapter 4.2).
[8] M. Hino, et al., Nucl. Instr. and Meth. A 529 (2004) 54.
[9] http://www.hmi.de/projects/ess/vitess/.
[10] G. Zsigmond, et al., Neutron News 13.4 (2002) 11.
[11] P. Thiyagarajan, et al., in: J. Suzuki, S. Itoh (Eds.), Proceedings of the ICANS-XV, JAERI Conference 2001–2002, Tsukuba, 2000, p. 454.
[12] J. Zhao, in: J. Suzuki, S. Itoh (Eds.), Proceedings of the ICANS-XV, JAERI Conference 2001–2002, Tsukuba, 2000, p. 466.
[13] R.K. Heenan, et al., in: F. Mezei, R. Eccleston (Eds.), Performance of a Suite of Generic Instruments on ESS—ESS Instrumentation Group Reports, ESS 115-01-T, Berlin, 2001, p. 71.
[14] A.V. Belushkin, S.A. Manoshin, J. Neutron Res. 10 (2002) 79.
[15] R. Gähler, et al., J. Phys. E 13 (1980) 546.
[16] K.C. Litrell, et al., Appl. Phys. A 74 (Suppl.) (2002) S1480.
[17] M. Arai, et al., in: G. Mank, H. Conrad (Eds.), Proceedings of the ICANS-XVI, FZ Jülich, Jülich, 2003, p. 157.
[18] B. Alefeld, et al., Physica B 234–236 (1997) 1052.